Analytical formulation for gravitation modeling of mass-heterogeneous bodies

Article *in* Journal of Geodesy · December 2022

DOI: 10.1007/s00190-022-01684-z

5 authors, including:

Wen-Yue Dai
Tsinghua University
2 PUBLICATIONS **0** CITATIONS
SEE PROFILE

Yang Yu
Beihang University (BUAA)
74 PUBLICATIONS **1,178** CITATIONS
SEE PROFILE

Bin Cheng
Tsinghua University
32 PUBLICATIONS **129** CITATIONS
SEE PROFILE

Hexi Baoyin
Tsinghua University
319 PUBLICATIONS **4,212** CITATIONS
SEE PROFILE

Analytical formulation for gravitation modeling of mass-heterogeneous bodies

Wen-Yue Dai[1], Yang Yu[2*], Bin Cheng[1], Hexi Baoyin[1] and Jun-Feng Li[1*]

[1]Tsinghua University, Beijing, 100084, China.
[2]Beihang University, Beijing, 100191, China.

*Corresponding author(s). E-mail(s): yuyang.thu@gmail.com; lijunf@tsinghua.edu.cn;

Abstract

An analytical gravity modeling formulation for heterogeneous bodies is developed in this paper, in which the compact closed formulation of gravitational potential and attraction is derived analytically. Using linear-interpolated density over finite element meshes, the formulation shows global convergence and consistent reliability in both exterior and interior, and on the interface. The contribution caused by arbitrary non-spherical shape and non-uniform mass distribution are considered separately in this method, which brings natural flexibility to gravity modeling. Benchmark tests are performed to verify the global convergence and reliability. A typical application to asteroid (25143) Itokawa is shown at the end of this paper, which proves the capacity and reliability of this method in gravity modeling of a practical irregularly-shaped heterogeneous asteroid.

Keywords: gravitation, celestial mechanics, asteroid

1 Introduction

The representation and computation of the gravity from given mass distribution are central problems in mathematical geodesy. For the construction of Earth's global gravitation model, the standard treatment is to express the

potential in terms of spherical harmonics [12]. The convergence of harmonics becomes worse as the field point gets closer to the Reference Sphere (RS), and inside the domain of RS, it becomes divergent. For a nearly spherical body like Earth, the spherical harmonics show good performance in efficiency of accuracy. However, the situation is different for small solar system bodies, e.g. comets and asteroids, whose shapes are usually highly non-spherical. The ellipsoidal harmonic expansion is proposed to solve this problem, which has a ellipsoidal divergence domain [18] and shows better convergence for highly irregular small bodies, but it still fails when the field point locates near the surface.

Both spherical and ellipsoidal harmonics are solution families of Laplace's equation

$$\Delta U(\mathbf{r}) = 0, \tag{1}$$

which assumes zero mass distribution in the concerned domain. Recently, Wei et al. [23] introduced the virtual boundary method to the Laplace-based gravitation modeling, and the new formulation shows convergence on the surface but fails in the interior. The zero-mass-distribution assumption can not be satisfied if the observation point is near the surface or in the interior of the body, and it is the origin of the non-negligible divergence of all Laplace-based methods.

Instead of considering the mathematical problems of a harmonic field, the solution to the divergence of Laplace-based methods is to return to the basic gravitation laws and calculate the gravitation directly. For instance, one need to solve the integral

$$\mathbf{f}(\mathbf{r}) = -\int_{\Omega} \rho(\mathbf{r}') \frac{\mathbf{r} - \mathbf{r}'}{\|\mathbf{r} - \mathbf{r}'\|^3} dV', \tag{2}$$

to obtain the gravitational attraction $\mathbf{f}$ of the small body Ω with a density distribution ρ. Here $\mathbf{r}$ and $\mathbf{r}'$ are the positions of the observation point and considered differential volume respectively. As high-resolution polyhedral shape models of many small bodies are obtained from recent space missions, it is convenient and practical to calculate the integral with a polyhedral region Ω.

For nearly homogeneous small bodies, a polyhedron Ω with constant density is a good approximation to calculate the gravity. Werner [24] and Werner et al. [25] developed an analytical closed-form formulation of the gravitation of homogeneous polyhedrons, which is now commonly used in small body dynamics [15, 19, 30]. Meanwhile, Petrović [17], Holstein [13], Tsoulis [21], D'Urso [3] and Conway [2] gave different equivalent formulations. All these formulations show global convergence and reliability (surface, exterior and interior of the bodies) in gravity modeling. Discussion on possible singularities can be found in Tsoulis et al. [22].

However, many small bodies are proved to be with heterogeneous structures, which break the homogeneous assumption in previous polyhedron model. Through investigation on the self-rotation status, Lowry et al. [16] confirmed

the heterogeneous interior of asteroid (25143) Itokawa. With impact analysis and the gravity model from NASA's Dawn spacecraft, Ermakov et al. [7] revealed the crust-mantle-core interior structure of (4) Vesta. And recently, Scheeres et al. [20] generated a heterogeneous layered structure model of (101955) Bennu with the gravity model obtained from analysis on the orbits of ejected particles. To treat the heterogeneous interior, Wittick et al. [26, 27] applied the mascon models to gravity modeling, but its computational consumption increases rapidly with the model resolution. Fukushima [9] proposed an approximate numerical method with series expansion of the density and regularized Newton kernels, but its physical meaning is not clear enough.

Back to the polyhedral approximation, Hansen [11] and D'Urso [4] gave gravity formulations for the polyhedron with a linearly varying density, which is the simplest case of heterogeneity. D'Urso et al. [5] extended these globally convergent formulations to polyhedrons with a polynomial density distribution. Considering that all continuous functions can be approximated by polynomial series, principally the D'Urso formulation is able to model nearly all the possible heterogeneous density. Yu et al. [29] developed a formulation based on the Finite Element (FE) mesh, which is directly the linear approximation of Equation (2) on a tetrahedral mesh frame. Different from polynomial approximation, the FEM-based methods are more capable to model complex geometry and density distribution. The Yu method shows reliability and extendibility, but this formulation would fail if the observation point was in a relatively thin layer near the surface of the body due to the singularity.

In this paper, an FE-mesh-based gravitation formulation is developed based on the linear FE mesh frame from Yu et al. [29] and the mathematical techniques applied by Werner [24] and Werner et al. [25]. With this new formulation, the heterogeneous mass distribution can be considered precisely, and the global convergence and extendibility/flexibility of the gravitation model are guaranteed. Additionally, the proposed formulation is naturally suitable to be migrated to the FE frame applied in the morphology and dynamics study on small bodies.

In Section 2, we present the analytical closed-form of our gravitational formula, together with a detailed derivation. In Section 3, results of benchmark tests are presented, which confirmed the global convergence and reliability numerically. In Section 4, we apply our methodology to the gravitation modeling of asteroid (25143) Itokawa. Finally, we offer a summary in Section 5.

2 A gravity formulation based on tetrahedral meshes

With a linear tetrahedral FE mesh frame (Figure 1a), the gravitation integral in Equation (2) can be approximately calculated through the linear

interpolation of gravity function [29]:

$$\mathbf{g}(\mathbf{r},\mathbf{r}') = -\rho(\mathbf{r}')\frac{\mathbf{r}-\mathbf{r}'}{\|\mathbf{r}-\mathbf{r}'\|^3}. \tag{3}$$

For example, the gravitational attraction would be

$$\mathbf{f}(\mathbf{r}) = \frac{1}{24}\sum_{k\in\text{Elements}} {J_k}^{-1} \sum_{j\in\text{Nodes}} \mathbf{g}(\mathbf{r},\mathbf{r}_j^k)\ , \tag{4}$$

in which the gravitation expressed as linear combination of node gravity $\mathbf{g}(\mathbf{r},\mathbf{r}_j^k)$, and J_k depends only on the geometry of the element k. Note the volume of element Ω_k as V^k, and 4 different facets as f_j $(j=1,2,3,4)$, of which outward unit normal vectors are $\mathbf{n}_j^k$. We have the analytical expression of J_k:

$$J_k = \frac{S_1^k S_2^k S_3^k}{27(V^k)^3}|(\mathbf{n}_1^k \times \mathbf{n}_2^k)\cdot\mathbf{n}_3^k|, \tag{5}$$

where S_j^k indicates the area of the facet f_j.

We note this method as LT-GI method (Linear-Tetrahedron-based Gravity Interpolation). LT-GI performs much better in convergence than the harmonic expansion approach when modeling highly irregular shaped bodies, because LT-GI shows divergence only in a thin layer close to the surface, while the RS (RE) of harmonic-based method can hardly fit the shape of the body. The divergence of LT-GI formulation origins from the singularity of the Newton kernels $1/\|\mathbf{r}-\mathbf{r}'\|$ and $1/\|\mathbf{r}-\mathbf{r}'\|^2$ at the considered position $\mathbf{r}'$, inducing this method also fails in the interior of the body.

The near-surface divergence in gravitation modeling is catastrophic in many situations, such as simulations of the surface dynamics of asteroids. In order to solve this divergence problem, we consider the interpolation of mass density ρ (we note the interpolation function as $\tilde{\rho}$) instead of the gravity function. For instance, the gravitational attraction expression is

$$\tilde{\mathbf{f}} = \sum_k \int_{\Omega_k} \tilde{\rho}^k \frac{\mathbf{r}-\mathbf{r}'}{\|\mathbf{r}-\mathbf{r}'\|^3} dV' = \sum_k \tilde{\mathbf{f}}^k\ , \tag{6}$$

in which $\tilde{\rho}^k$ is the linear interpolation on element Ω_k, $\tilde{\mathbf{f}}$ indicates the contribution from Ω_k, and we have $\Omega = \bigcup_k \Omega_k$. This gravitation formulation is supposed to show global convergence (even in the interior of the body), because it is related to a realistic system with continuous mass density distribution $\tilde{\rho}$ rather than a linear approximate solution of the gravitation integral. Theoretically, this formulation erases the singularity of the Newton kernels by integrating, and it is a higher-level approximation of the real gravitation of concerned celestial body than LT-GI approximation. LT-DI is supposed to be consistent with LT-GI result when the observation position is not close to the surface.

We note this new global approach as LT-DI method (Linear-Tetrahedron-based and Density Interpolation), and it is the focus of this work. In the following, an analytic closed expression of gravitation approximation based on this approach is presented.

2.1 Gravitational Attraction

2.1.1 Linear interpolation on elements

Note the interpolated density function on a single element Ω_k as

$$\tilde{\rho}^k(\mathbf{r}) = \mathbf{a}^k \cdot \mathbf{r} + b^k \ , \tag{7}$$

in which $\mathbf{a}^k$ and b^k can be easily conducted from the linear interpolation [29]. And we can similarly give the interpolated density on a single facet s:

$$\tilde{\rho}_s(\mathbf{r}) = \mathbf{a}_s \cdot \mathbf{r} + b_s, \tag{8}$$

in which the parameters $\mathbf{a}_s$ and b_s can also be obtained from the global interpolation. Explicitly, given the density value ρ_j^k on node $j (j = 1, 2, 3, 4)$ of the element Ω_k, we have

$$\mathbf{a}^k = -\sum_j \frac{S_{\bar{j}}^k}{3V^k} \rho_j^k \mathbf{n}_{\bar{j}}^k \text{ and } b^k = \sum_j \frac{S_{\bar{j}}^k}{3V^k} \rho_j^k (\mathbf{n}_{\bar{j}}^k \cdot \mathbf{r}_j^k). \tag{9}$$

Here $\mathbf{r}_j^k$ indicates the position vector of node j. The subscript $\bar{j}$ means the opposite facet of node j, $\mathbf{n}_{\bar{j}}^k$ and $S_{\bar{j}}^k$ are the outward unit normal vector and the area of this facet respectively. As for $\mathbf{a}_s$ and b_s, find the element Ω_l, of which s is the facet, and we have $\mathbf{a}_s = \mathbf{a}^l$ and $b_s = b^l$.

2.1.2 Surface part and interior part

The gravitational attraction can be directly calculated by solving a volume integral of Equation 2. We can get the gravitation through calculating all the contribution from elements as Equation 6 shows. According to the discussion on the gravitation of polyhedron with linear density from D'Urso [4], the contribution from elements can be easily written as a closed form. However, this method would cause repetitive computation at facets or edges, etc. To overcome this problem, we separate the volume integral into two parts: (1) The surface part, which consists of surface integrals on the surface of the considered celestial body; (2) The interior part, which is the sum of volume integrals over single element related to the gradient of density.

First, Gauss's theorem (the divergence theorem) [14] is applied to reveal the contribution from the surface (surface part). Given the body Ω, Gauss's theorem ensures that for any smooth vector function $\mathbf{h}(\mathbf{r})$, we have

$$\int_{\Omega} \nabla \cdot \mathbf{h} dV = \int_{\partial\Omega} \mathbf{h} \cdot \mathbf{n} dA, \tag{10}$$

where the vector $\mathbf{n}$ indicates the outward normal unit vector on the surface $\partial\Omega$ and dA is the differential area element. Let $\mathbf{R} = \mathbf{r}' - \mathbf{r}$, and the integral of gravitational attraction is translated to

$$\mathbf{f}(\mathbf{r}) = \int_{\Omega} \rho \frac{\mathbf{R}}{R^3} dV = -\int_{\Omega} \left[\nabla_{\mathbf{R}} \left(\frac{\rho}{R} \right) - \frac{1}{R} \nabla_{\mathbf{R}} \rho \right] dV, \tag{11}$$

and here $\nabla_{\mathbf{R}}$ indicates $\partial/\partial\mathbf{R}$. Using Gauss's theorem over the polyhedron volume Ω, then we have

$$\mathbf{f}(\mathbf{r}) = -\int_{\partial\Omega} \frac{\rho}{R} \mathbf{n} dA + \int_{\Omega} \frac{1}{R} \nabla_{\mathbf{R}} \rho dV, \tag{12}$$

The surface part is

$$\mathbf{f}_{\text{sur}} = -\int_{\partial\Omega} \frac{\rho}{R} \mathbf{n} dA, \tag{13}$$

and the interior part is

$$\mathbf{f}_{\text{in}} = \int_{\Omega} \frac{1}{R} \nabla_{\mathbf{R}} \rho dV. \tag{14}$$

Considering the linear interpolation of density, the surface part is

$$\mathbf{f}_{\text{sur}} = -\sum_{s \in F\Omega} \mathbf{n}_s \int_{s} \left[\mathbf{a}_s \cdot \frac{\mathbf{R}}{R} + (\mathbf{a}_s \cdot \mathbf{r} + b_s) \frac{1}{R} \right] dA, \tag{15}$$

which shows the influence of the value of density on surface to the total gravity, and here we use $F\Omega$ to note the set of all facets of polyhedron Ω. The interior part is

$$\mathbf{f}_{\text{in}} = \sum_{k} \mathbf{a}^k \int_{\Omega_k} \frac{1}{R} dV, \tag{16}$$

suggesting the effect of density heterogenicity in gravity can be presented as a volume integral of density gradient.

2.1.3 Surface Integrals over Polygon Area

All the polygon surface integrals appearing in above result of $\mathbf{f}_{\text{sur}}$ and $\mathbf{f}_{\text{in}}$ are only related to function $1/R$ and $\mathbf{R}/R$. In this part, we will generally discuss the integral of these 2 functions over a polygon region f with a unit normal vector $\mathbf{n}_f$.

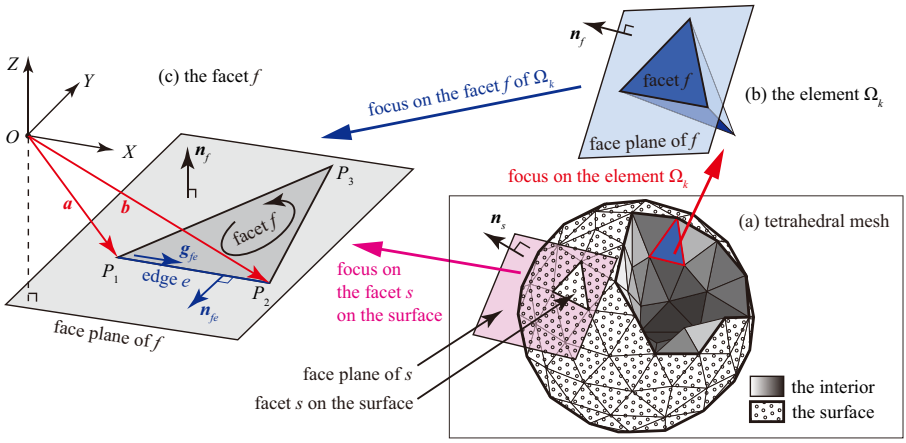

Fig. 1 Geometry of the tetrahedron mesh, the elements and the facets in this paper: (a) the interior and the surface of the mesh; (b) the tetrahedron element and its facets; (c) the geometry of the facet and its edges.

We firstly consider the integral of function $\frac{1}{R}$, which Werner et al. [25] have thoroughly investigated. Generally, we have

$$\int_f R^{-1} dA = \sum_{e \in Ef} (\mathbf{n}_{fe} \cdot \mathbf{R}_{fe}) L_{fe} - d_f \omega_f, \tag{17}$$

in which Ef indicates the set of all the edges of polygon f (the directions of all these edges satisfy right-hand rule, shown in Figure 1), $\mathbf{n}_{fe}$ indicates the outward normal vector at edge e (on the face plane of f), $\omega_f = \int_f \frac{\mathbf{n} \cdot \mathbf{R}}{R^3}$ is the signed solid angle subtended by the planar region f, and L_{fe} is

$$L_{fe} = \ln \frac{a + b + e}{a + b - e}. \tag{18}$$

More detail about these vectors and directions is shown in Figure 1.

The integral of $\frac{\mathbf{R}}{R}$ can be well calculated using the technique from D'Urso [4], which means we can separate the function $\frac{\mathbf{R}}{R}$ into 2 parts:

$$\frac{\mathbf{R}}{R} = \frac{d_f \mathbf{n}_f}{R} + \frac{\mathbf{R}_\parallel}{\left(d_f^2 + R_\parallel^2\right)^{1/2}}, \tag{19}$$

in which $d_f = (\mathbf{R}_f \cdot \mathbf{n}_f)\mathbf{n}_f$ is constant for any point $\mathbf{R}_f$ on the face plane and $\mathbf{R}_\parallel = \mathbf{R} - d_f \mathbf{n}_f$. Note that the relation $R^2 = d_f^2 + R_\parallel^2$ is applied in the equation above. The integral of $\frac{1}{R}$ has been given above, $d_f \mathbf{n}_f$ is constant on the facet

f and

$$\int_f \frac{\mathbf{R}_{\parallel}}{\left(d_f^2 + R_{\parallel}^2\right)^{1/2}} dXdY \tag{20}$$

is a pure 2D problem which can be easily solved with Gauss's theorem in planar region. Through simple calculation, we can give the result:

$$\begin{aligned}\int_f \frac{\mathbf{R}}{R} dA =& d_f \mathbf{n}_f \left[\sum_{e\in Ef} (\mathbf{n}_{fe}\cdot\mathbf{R}_{fe}) L_{fe} - d_f\omega_f\right] \\ &+ \sum_{e\in Ef} \frac{\mathbf{n}_{fe}}{2}\left(H_{fe} + D_{fe}^2 L_{fe}\right)\end{aligned} \tag{21}$$

in which D_{fe} is

$$D_{fe}^2 = d_f^2 + \left(\mathbf{R}_{fe}\cdot\mathbf{g}_{fe}\right)^2 \ , \ \mathbf{g}_{fe} = \frac{\mathbf{b}-\mathbf{a}}{\|\mathbf{b}-\mathbf{a}\|}, \tag{22}$$

H_{fe} is

$$H_{fe} = (b\mathbf{b} - a\mathbf{a})\cdot\mathbf{g}_{fe}, \tag{23}$$

and here $\mathbf{R}_{fe}$ can be any chosen point located at the edge $e \in Ef$.

2.1.4 The total gravitational attraction

The closed form of the surface part can be easily obtained with the results of $\int_f \frac{\mathbf{R}}{R} dA$ and $\int_f R^{-1} dA$:

$$\begin{aligned}\mathbf{f}_{\text{sur}} =& -\sum_{s\in F\Omega} \rho_s \mathbf{n}_s \left[\sum_{e\in Es} (\mathbf{n}_{se}\cdot\mathbf{R}_{se}) L_{se} - d_s\omega_s\right] \\ &- \frac{1}{2}\sum_{s\in F\Omega} \mathbf{n}_s\mathbf{a}_s \cdot \sum_{e\in Es} \mathbf{n}_{se}\left(H_{se} + D_{se}^2 L_{se}\right).\end{aligned} \tag{24}$$

in which we note $\rho_s = \mathbf{a}_s\cdot(d_s\mathbf{n}_s + \mathbf{r}) + b_s$. As mentioned, the volume integrals appearing in the interior part are the same as that from homogeneous polyhedron potential, and thus, the interior part can be derived from the result from Werner [24], Werner et al. [25], we have the closed form of interior part:

$$\begin{aligned}\mathbf{f}_{\text{in}} =& \sum_k \mathbf{a}^k U_h^k \\ =& \frac{1}{2}\sum_k \mathbf{a}^k \sum_{f\in F\Omega_k} d_f \left[\sum_{e\in Ef} (\mathbf{n}_{fe}\cdot\mathbf{R}_{fe}) L_{fe} - d_f\omega_f\right],\end{aligned} \tag{25}$$

and here U_h^k indicates the potential of a homogeneous polyhedron element Ω_k with density $\rho_0 = 1$, which can be easily calculated with the results of Werner [24], Werner et al. [25].

The total gravitational attraction is given by

$$\mathbf{f} = \mathbf{f}_{\text{in}} + \mathbf{f}_{\text{sur}}. \tag{26}$$

Like the Werner formulation, most of the calculation needed here is dependent only on the geometry of the tetrahedral mesh, which doesn't require refresh as the time integration. As a degeneration, if the density ρ was constant, the interior part would be zero, and the gravitational attraction would be

$$\mathbf{f} = \rho \sum_{s \in F\Omega} \left[\mathbf{n}_s \mathbf{n}_s \cdot \mathbf{R}_s \omega_s - \sum_{e \in Es} (\mathbf{n}_s \mathbf{n}_{se} \cdot \mathbf{R}_{se}) L_{se} \right], \tag{27}$$

which is consistent with the homogeneous polyhedron formulation from Werner [24], Werner et al. [25], and the total gravity was determined only by the surface (shape) of the body.

2.2 Gravitational Potential

The gravitation potential can be obtained by solving the volume integral

$$U(\mathbf{r}) = \int_{\Omega} \frac{\rho}{R} dV \ . \tag{28}$$

With Gauss's theorem we can transform the integral to

$$U(\mathbf{r}) = \frac{1}{2} \int_{\partial\Omega} \rho \frac{\mathbf{R}}{R} \cdot \mathbf{n} dA - \frac{1}{2} \int_{\Omega} \frac{\mathbf{R}}{R} \cdot (\nabla_{\mathbf{R}} \rho) \, dV, \tag{29}$$

the surface part is

$$U_{\text{sur}} = \frac{1}{2} \int_{\partial\Omega} \rho \frac{\mathbf{R}}{R} \cdot \mathbf{n} dA \ , \tag{30}$$

and the interior part is

$$U_{\text{in}} = -\frac{1}{2} \int_{\Omega} \frac{\mathbf{R}}{R} \cdot (\nabla_{\mathbf{R}} \rho) \, dV = -\frac{1}{2} \sum_k \mathbf{a}^k \cdot \mathbf{u}^k \ . \tag{31}$$

In our linear tetrahedron mesh system, the surface part is

$$\begin{aligned} U_{\text{sur}} =& \frac{1}{2} \sum_{s \in F\Omega} d_s \int_s \frac{\rho}{R} dA \\ =& \frac{1}{2} \sum_{s \in F\Omega} d_s \left[\mathbf{a}_s \cdot \int_s \frac{\mathbf{R}}{R} dA + (\mathbf{a}_s \cdot \mathbf{r} + b_s) \int_s \frac{1}{R} dA \right]. \end{aligned} \tag{32}$$

in which $\mathbf{n}_s$ indicates the normal vector of the facet s, and d_s is constant on the facet s. And the interior part is

$$U_{\text{in}} = -\frac{1}{2} \sum_k \mathbf{a}^k \cdot \mathbf{u}^k, \tag{33}$$

in which $\mathbf{u}^k = \int_{\Omega_k} \frac{\mathbf{R}}{R} dV$. Notice that $\frac{\mathbf{R}}{R} = \nabla_{\mathbf{R}} R$, then we have

$$\mathbf{u}^k = \sum_{f \in F\Omega_k} \mathbf{n}_f^k \int_f R dA \ . \tag{34}$$

The integral of $\mathbf{R}/R$ and $1/R$ has been solved above, what remained is the integral of R. By considering this problem in a Cartesian coordinates system $OXYZ$, in which the OXY plane is parallel to the planar region f and $\mathbf{R} = (X, Y, Z)$, and noticing an identical relation

$$\frac{\partial}{\partial X}(RX) + \frac{\partial}{\partial Y}(RY) = 3R - \frac{Z^2}{R}, \tag{35}$$

we can reach to the result

$$\int_f R dA = \frac{1}{6} \sum_{e \in Ef} (\mathbf{n}_{fe} \cdot \mathbf{R}_{fe}) \left[H_{fe} + (D_{fe}^2 + 2d_f^2) L_{fe} \right] - \frac{1}{3} d_f^3 \omega_f. \tag{36}$$

With the discussions above, the gravitational potential of the piecewise linear system can be represented as closed form. According to Equation (32) and (33), we have the analytical closed forms of $\mathbf{u}^k$ and U_{sur}:

$$\mathbf{u}^k = \sum_{f \in F\Omega_k} \frac{\mathbf{n}_f^k}{6} \left\{ \sum_{e \in Ef} (\mathbf{n}_{fe} \cdot \mathbf{R}_{fe}) \left[H_{fe} + (D_{fe}^2 + 2d_f^2) L_{fe} \right] - 2d_f^3 \omega_f \right\}, \tag{37}$$

$$\begin{aligned} U_{\text{sur}} =& \frac{1}{2} \sum_{s \in F\Omega} d_s \rho_s \left[\sum_{e \in Es} (\mathbf{n}_{se} \cdot \mathbf{R}_{se}) L_{se} - d_s \omega_s \right] \\ &+ \frac{1}{4} \sum_{s \in F\Omega} d_s \mathbf{a}_s \cdot \sum_{e \in Es} \mathbf{n}_{se} \left(H_{se} + D_{se}^2 L_{se} \right). \end{aligned} \tag{38}$$

Therefore, the closed form of gravitational potential can be given with above 2 results and the definition:

$$U = U_{\text{in}} + U_{\text{sur}}. \tag{39}$$

The interior part would be zero if the density is constant, and by calculating the surface part we could have

$$U = \frac{1}{2} \rho \sum_{s \in F\Omega} \left\{ - (\mathbf{R}_s \cdot \mathbf{n}_s \mathbf{n}_s \cdot \mathbf{R}_s) \, \omega_s + \sum_{e \in Es} (\mathbf{R}_{se} \cdot \mathbf{n}_s \mathbf{n}_{se} \cdot \mathbf{R}_{se}) L_{se} \right\}, \tag{40}$$

which is consistent with Werner's result [24, 25].

3 Numeric implement and benchmark tests

3.1 Benchmark tests

Two benchmark examples are designed to validate the capacity of the LT-DI method: (a) homogeneous spheroid; (b) spheroid with a spherically symmetric mass distribution. The reason to choose spheroid examples rather than irregular shaped ones is to get simple analytical truth and avoid the influence of orientation. According to Section 2, the LT-DI formulation degenerates to the Werner formulation when modeling homogeneous polyhedrons, which means that the equivalence of these formulations in homogeneous situations is naturally given. In the homogeneous example, the LT-GI and Werner (LT-DI) results are compared to show that the singularity appearing in LT-GI method is erased by integrating in Werner (LT-DI) method. The heterogeneous example shows the capacity and reliability of LT-DI method when modeling systems with heterogeneous mass distribution, which is beyond the capacity of the Werner method.

In this work, the unit of length is m and the unit of density is kg/m^3. For simplicity, the unit will be omitted in the following. A spheroid, of which the radius is $R = 50$ and the center locates at $O = (0, 0, 0)$, is considered in this section, and all the spheroid examples are generated by varying their mass distributions. Only the results of gravitational attraction are discussed in this section and following.

The relative element size $\alpha = \frac{l}{L}$ describes the fineness of the mesh, where l is the characteristics element size (for instance, the max element size) and L indicates the size of the body (the diameter of the spheroid). The tetrahedral mesh with smaller α is able to describe the shape more finely and fit the density distribution better. A series of tetrahedron FE mesh systems with different

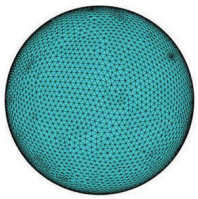

Mesh 1	
Number of nodes	29210
Number of elements	162263
Max element size	3.00
Min element size	1.50
α	0.03

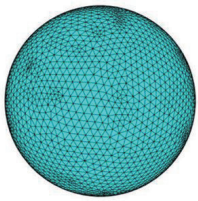

Mesh 2	
Number of nodes	12882
Number of elements	69652
Max element size	4.00
Min element size	2.00
α	0.04

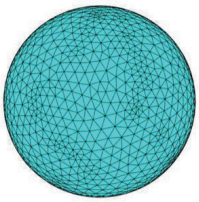

Mesh 3	
Number of nodes	4274
Number of elements	21643
Max element size	6.00
Min element size	3.00
α	0.06

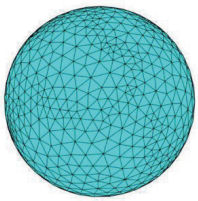

Mesh 4	
Number of nodes	2002
Number of elements	9573
Max element size	8.00
Min element size	4.00
α	0.08

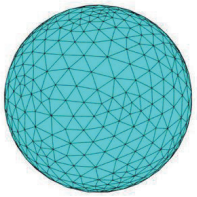

Mesh 5	
Number of nodes	1123
Number of elements	5107
Max element size	10.00
Min element size	5.00
α	0.10

Parameters of the spheroid	
Radius	50
Center	(0, 0, 0)

Fig. 2 Tetrahedron mesh system series (Mesh 1 to Mesh 5) generated for benchmark test, of which the key parameters are shown in the tables.

fineness is generated (Figure 2) to deploy LT methods on this spheroid. To discover the performance of GI and DI methods, the relative error function

$$\mathrm{RelErr}(\cdot) = \left\| \frac{\text{Approximate value} - \text{True value}}{\text{True value}} \right\| \tag{41}$$

is introduced, which evaluates the relative deviation of calculation result (approximate value) from the truth.

3.1.1 Homogeneous spheroid

The homogeneous spheroid example is obtained by setting a constant density of $\rho_0 = 1$, and the true gravitational field can be easily analytically given as

$$\mathbf{f}_{\mathrm{truth}}(\mathbf{r}) = \begin{cases} -\frac{4}{3}\pi\rho_0 R^3 \frac{\mathbf{r}}{r^3}, & r \geq R \\ -\frac{4}{3}\pi\rho_0 \mathbf{r}, & r < R \end{cases}. \tag{42}$$

It is necessary to demonstrate that the choice to set $\rho_0 = 1$ do not influence the investigation on the capacity of concerned methods. From Equation 2 we know that the original problem of calculating gravity is linear for the density distribution. And this linearity is inherited in all concerned formulations in this work. The linearity of the problem and the calculation formulations leads to the scale-invariance of relative error of gravity g to the density, which means that

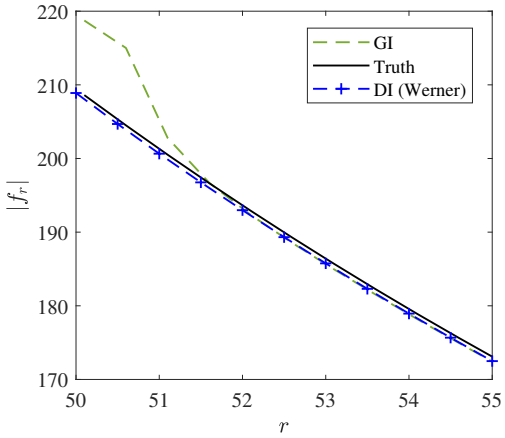

Fig. 3 The absolute value of gravitational attraction in radial direction, from the truth, GI and DI (Werner) result, respectively. The deviation of GI result from the truth is significant near the surface ($R = 50$).

for any possible density distribution ρ and any $k > 0$, we have $\mathrm{RelErr}(g)[\rho] = \mathrm{RelErr}(g)[k\rho]$. Here $\mathrm{RelErr}(g)[\rho]$ indicates the relative error of g calculated from the density distribution ρ. This result suggest that the scale of density ρ do not affect our final conclusion on the performance of formulations, except the rounding error of computer is considered. Therefore, to set $\rho_0 = 1$ is both convenient and general in this homogeneous example.

Figure 3 shows the gravitational attraction generated from Mesh 1, and the deviation between the truth of gravitational attraction and the LT-GI calculation result is significant in a thin layer (with a thickness of $d \sim 3$, $d/R \sim 10^{-2}$) close to the surface, while the DI result fits the truth much better. According to Section 2, the deviation of GI is mainly induced by singularity of the Newton kernel (detailed discussion is given in Section 3.2). As discussed above, in this case, because of the zero-valued gradient of density, the LT-DI formulation is equivalent to Werner's homogeneous polyhedron formulation, which has been proved to be a precise and powerful technique in small body dynamics.

Figure 4a shows $\mathrm{RelErr}(\mathbf{f})$ of the GI and DI modeling results in this homogeneous example with different mesh fineness. The relative deviations curve nearly shows distance independence when applying DI method, which suggests the global convergence of DI modeling. Contrarily, the $\mathrm{RelErr}(\mathbf{f})$ curve of GI results oscillates remarkably in a thin layer close to the surface, suggesting the divergence of GI modeling near the surface. Although the thickness of this divergence layer decrease with smaller α, the singularity near the surface can not be erased when applying LT-GI.

Yu [28] suggests that the deviation between Werner's polyhedron result and the truth is mainly caused by the difference between polyhedron model and

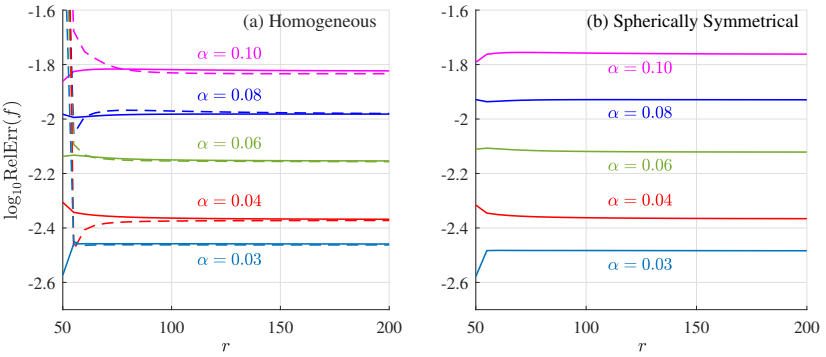

Fig. 4 (a) The relative error of both GI result (dash) and DI (Werner) result (solid) on homogeneous spheroid situation, generated from different mesh system. (b) The relative error of DI result on heterogeneous situation based on different mesh systems.

the real shape, and this deviation is essential and unavoidable when deploying polyhedron methods. This idea of essential deviation is correct in our FE framework, that is, the essential deviation is from the difference of the tetrahedron system from the true 3D morphology of small celestial body. In this case, the essential deviation of polyhedron method and our FE method is equivalent, which is only dependent with the shape. In this case, the GI and DI $\mathrm{RelErr}(f_r)$ rapidly overlap outside the GI divergence layer, and finer FE mesh leads to lower DI deviation. It shows that the deviation of DI result is almost the essential deviation when deploying an FE mesh frame.

3.1.2 Heterogeneous spheroid

A series of heterogeneous spheroid examples shows the capacity of DI method to model heterogeneous systems, which the Werner method is not able to deal with. Specifically, we consider a spheroid with a spherically symmetrical mass distribution

$$\rho(r) = \rho_0 + \rho_v(1 - r/R), \tag{43}$$

in which R represents the radius of spheroid ($R = 50$), ρ_0 is the background density, and ρ_v is a parameter controlling the variation of the distribution. Therefore, the truth of gravitational attraction is

$$\mathbf{f}_{\mathrm{truth}}(\mathbf{r}) = \begin{cases} -\left(\frac{4}{3}\pi\rho_0 R^3 + \frac{1}{3}\pi\rho_v R^3\right)\frac{\mathbf{r}}{r^3}, & r \geq R \\ -\frac{4}{3}\pi\rho_0\mathbf{r} - \frac{4}{3}\pi\rho_v\left(1 - \frac{3r}{4R}\right)\mathbf{r}, & r < R \end{cases}. \tag{44}$$

The reason to choose this spherically symmetric density distribution is to ensure that a simple analytical solution of the truth value can be obtained, and our analysis on the results is not related to the considered orientation. Both conveniently and generally, the background density is set to be $\rho_0 = 1$, for the same reason demonstrated in Section 3.1.1. Additionally, the set distribution

is heterogeneous everywhere in the spheroid, and we set $\rho_v = 1$ that makes the variation of the density is relatively large ($\rho_v/\rho_0 = 1$). We suppose that this simple distribution is heterogeneous enough to show the capacity of LT-DI.

Figure 4b shows the DI modeling error based on meshes with different α (different mesh fineness). As expected, finer meshes lead to smaller DI error. Consistent with the homogeneous example, RelErr($\mathbf{f}$) of DI results is well stable on a certain order, suggesting good global convergence.

Discussing these error results from another view point is helpful to re-confirm the reliability of LT-DI. In heterogeneous cases, the difference between the true density and the interpolation contributes to the essential deviation, that means

$$\text{Essential deviation} \sim m\frac{\delta\rho}{\rho} + \frac{n}{3}\frac{\delta V}{V}. \tag{45}$$

Here $\delta\rho/\rho$ is the relative error of ρ from interpolating, $\delta V/V$ is the relative error of volume, and m and n are parameters ~ 1. Considering that $V \sim L^3$ and $\delta L \sim l$, we have

$$\text{Essential deviation} \sim m\frac{\delta\rho}{\rho} + n\frac{\delta L}{L} \sim m\frac{\delta\rho}{\rho} + n\alpha. \tag{46}$$

In this heterogeneous example, we find that the density relative error $\delta\rho/\rho \sim 0.01$ for all appeared values of α (0.1, 0.08, 0.06, 0.04 and 0.03). According to Equation 46, in this case we have a conservative estimation of the essential deviation, that the order of magnitude of essential deviation is 0.01 to 0.1. This estimation is consistent with the results in Figure 4 that the errors ~ 0.01 for all considered α.

3.2 Remarks

With an FEM tetrahedron frame, our LT-DI methods extend the capability of polyhedron method, and a closed analytical form of the gravitational field of a system with heterogeneous mass distribution is given. However, sometimes traditional LT-GI is a better choice in certain situation. It is necessary to summarize the advantages and disadvantages of these 2 LT methods:

1. LT-GI is based on a simple linear interpolation, but expressions from LT-DI contain many complex geometric quantities. The structure of LT-GI method is far simpler than that of LT-DI, which means LT-GI method is easier to be deployed and requires less computation resource.
2. The Newton kernels $1/r$ and $1/r^2 \to +\infty$ when $r \to 0$, that means the result of LT-GI formulation fails (the gravity would go infinite) when the position is close to a node, while LT-DI method shows global convergence. Therefore, although the result of LT-GI method is correct when the position is not near the surface of the small body, the result would be divergent if the position entered a thin layer close to the surface.
3. LT-GI method fails inside the body due to the divergence, while LT-DI remains convergence inside the body. Figure 5 shows the LT-DI modeling

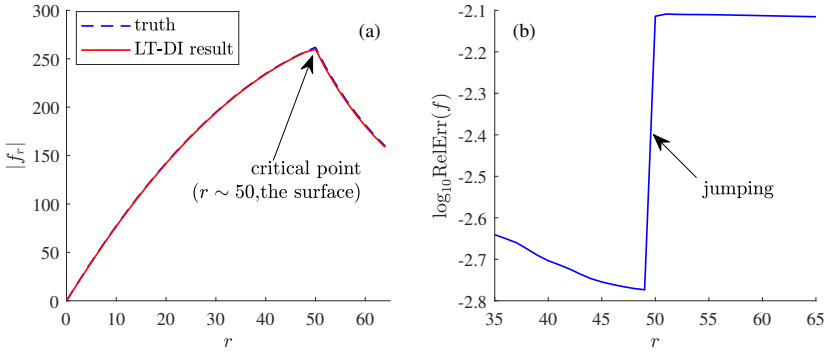

Fig. 5 DI results of gravitational attraction based on Mesh 3 ($\alpha = 0.06$), involving both interior and exterior areas: (a) The absolute value of gravitational attraction in the radial direction, DI results comparing with the truth; (b) The relative errors.

result involving areas inside the body, showing the reliability of LT-DI both inside and outside the body. The jumping of relative error (Figure 5b) is due to that the gravitational gradient (Figure 5a shows a critical point) is not continuous on the surface, and it suggests that the performance on surface is important in gravitation modeling.

In summary, LT-DI is globally convergent and more reliable, but requires more computational resource. Contrarily, LT-GI is not globally convergent, but it is simple and lower computational cost. Therefore, if dynamics near or on the surface was involved, the LT-DI method would be the only choice for its global convergence. For situations that require the interior gravitational field, such as the computation of gravitational interaction energy

$$W = \frac{1}{2}\int_{\Omega} \rho(\mathbf{r})U(\mathbf{r})dV, \tag{47}$$

LT-DI approach also seems the only choice among all LT methods. When considering orbit dynamics in the vicinity of small bodies, LT-GI is an efficient choice since the divergence of this method can be ignored because of the object is not close to the surface.

4 Application to asteroid (25143) Itokawa

Asteroid (25143) Itokawa was visited by JAXA's Hayabusa spacecraft in 2005, with a precise high-detailed shape model obtained in this visit [10]. Itokawa's shape is highly irregular (Figure 6), which can be divided as two parts: the body and the head. And it has been confirmed to be a typical rubble pile with heterogeneous interior mass distribution [16]. Itokawa's total mass measured by the spacecraft is approximately $M \sim 3 \times 10^{10}$kg, and its average density is about 1950 kg/m^3 [1]. We apply the LT-DI method on Itokawa to show its capacity on realistic situations. Specifically, we focus on the gravitational

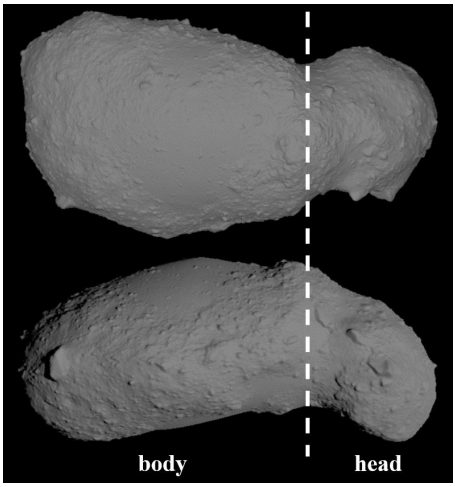

Fig. 6 Asteroid (25413) Itokawa's shape model from Hayabusa mission [19]. The body part and the head part of Itokawa are shown in the figure.

attraction on the surface of Itokawa. Because the actual interior mass distribution of Itokawa is unknown, the following discussion is based on an artificial interior mass tumor model and the multi-part models from Lowry et al. [16].

4.1 Itokawa with an interior mass tumor

In this section, we discuss the capacity and reliability of LT-DI method in a realistic asteroid situation with an artificial mass tumor model.

The mass tumor model is obtained by add an extra spherically symmetrical mass tumor on the (homogeneous) background density of $\rho_0 = 1950$ kg/m^3, and here we set

$$\rho(\mathbf{r}) = \begin{cases} \rho_0 + \frac{4M_T}{\pi^2 R_T^3}\sqrt{1 - \frac{\|\mathbf{r}-\mathbf{r}_T\|^2}{R_T^2}}, & \text{if } \|\mathbf{r}-\mathbf{r}_T\| \le R_T \\ \rho_0, & \text{if } \|\mathbf{r}-\mathbf{r}_T\| > R_T \end{cases}, \tag{48}$$

in which M_T, R_T and $\mathbf{r}_T$ indicate the tumor total mass, the tumor radius and the position of the center of the tumor, respectively. The tumor mass M_T is set to be 9×10^9 kg, because we believe the mass ratio $M_T/M \sim 0.3$ is acceptable to make the effect of tumor on gravity relatively significant. The tumor is added to the head part. To assure that the tumor is contained by the body part and get a tumor as large as possible, we set $R_T = 0.08$ km and $\mathbf{r}_T = (-0.15, 0, -0.02)$ (km).

The true gravity of the mass tumor can be analytically given as

$$\mathbf{f}_{\text{truth}} = \mathbf{f}_{\text{homo}} - M_T \frac{\mathbf{r}-\mathbf{r}_T}{\|\mathbf{r}-\mathbf{r}_T\|^3} \tag{49}$$

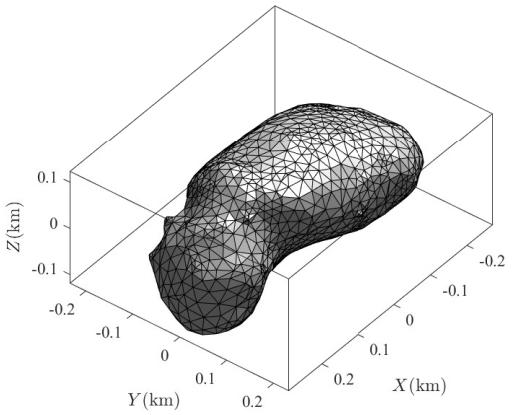

Fig. 7 The 72k-element mesh generated from Itokawa's shape model.

Table 1 Parameters of the tetrahedron mesh system.

parameter	value
node num.	14,517
elem. num.	72,214
max elem. size (km)	0.0144
min elem. size (km)	0.0072
α	~ 0.05

where $\mathbf{f}_{\text{homo}}$ indicates the gravitational attraction generated from homogeneous Itokawa with density of $\rho_0 = 1950\text{kg/m}^3$. In this work, $\mathbf{f}_{\text{homo}}$ is calculated with the LT-DI (Werner) formulation.

The DI computation is completed on a 72,000-elements tetrahedron mesh system (Figure 7, and the parameters shown in Table 1). We calculate $\mathbf{f}_{\text{homo}}$ with the same mesh, so that the deviations caused by the shape approximation, which is contained only in $\mathbf{f}_{\text{homo}}$, are equal in both heterogeneous DI result and the truth we set in Equation 49. And it means errors occurring in this case are mainly induced by the $(\delta\rho/\rho)$ term in Equation 46. Since the background density ρ_0 is constant, the $(\delta\rho/\rho)$ term is related to the mass tumor.

Figure 8 shows the distribution of gravitational attraction on the surface and the relative error RelErr($\mathbf{f}$). The relative error ranges up to $\sim 10^{-2}$ in certain regions on the "top" of the body part, which are closer to the mass tumor than anywhere else on the surface, and the maximum RelErr($\mathbf{f}$) is 0.0070. However, for other areas on the surface, the error is usually $10^{-3} \sim 10^{-4}$. On the head part, which is the farthest to the mass tumor, RelErr($\mathbf{f}$) is nearly constantly $\sim 10^{-4}$ or below. This difference in RelErr($\mathbf{f}$) can be clearly explained as that the $(\delta\rho/\rho)$ term (the deviation from density interpolating) is stronger in areas closer to the tumor, and weaker in areas further from the tumor.

In summary, LT-DI method shows good capacity and reliability in realistic asteroid situations (with highly irregular shape and heterogeneous density) as

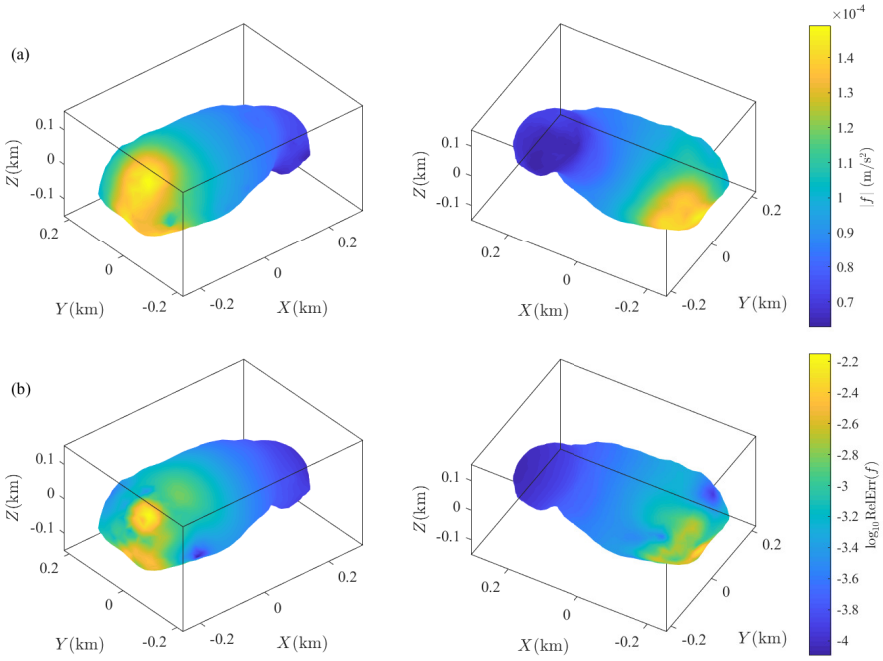

Fig. 8 (a) DI result of the gravitational attraction (here we shows $\|\mathbf{f}\|$) on Itokawa's surface, and here we set $G = 6.67 \times 10^{-11}$ kg $\cdot$ m^3/s^2. (b) Relative error of DI result on Itokawa's suface.

its performance in spheroid benchmark tests above. In the following section, we apply LT-DI method with a more realistic density distribution model to understand more details of Itokawa's surface gravitation.

4.2 Local slopes of Itokawa

The local slopes on Itokawa's surface, which shows the influences of gravity to the surface topography, is investigated in this section. We apply 2 interior mass models from Lowry et al. [16] respectively in our discussion: the head-body model (HB model) and the head-neck-body model (HNB model, with a compressed higher-density neck), shown as Figure 9. These 2 mass models are based on different assumptions on the origin of Itokawa, The DI computation is completed with the mesh system shown in Figure 7. Importantly, in this case the rotational acceleration cannot be ignored, and thus we calculate the rotation effects with a center-shift model from Lowry et al. [16].

Figure 10 shows the local slope distribution on the surface of Itokawa, based on both HB and HNB model. The maximum slope is 37.5° for HB model and is 50.8° for HNB, showing a remarkable difference about 15°. For both these 2 interior models, the maximum slope appears on the southern surface of head part, and on the side of head the slope is apparently large (slope $\geq$ 25° for HB model, and $\geq$ 30° for HNB model). Near both the south pole and the

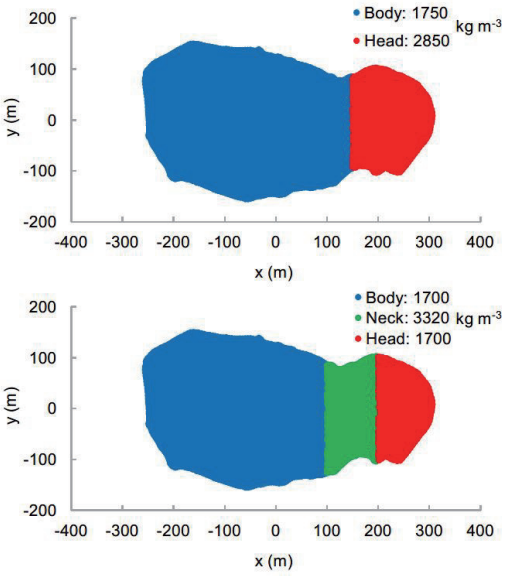

Fig. 9 Mass distribution models of Itokawa from Lowry et al. [16]. *Upper Panel* - The body-head model (HB model). *Lower Panel* - The head-neck-body model (HNB model).

north pole the surface slope is lower than 5°, which is consistent with the large plains in the vicinity of the poles of Itokawa. All these results above show good agreement with the observation of Hayabusa spacecraft: the side of head part is rough and rocky, covered by big rocks, which coincides with large slope; the areas with lower slope coincides with the existence of large-scale plains covered by smooth regolith, such as Sagamihara on the northern pole and Muses Sea on the southern pole [8].

Additionally, Figure 10c shows that the difference $\Delta\phi = \phi_{HNB} - \phi_{HB}$ is nearly 0° on surface of the body part, while difference ranging up to $\sim 15°$ occurs on surface of the head part, especially on the side face. It means, when considering the HB-like or HNB-like mass distribution mode, the slopes on surface of the head part is more sensitive to the structure of mass model than other areas. Therefore, measuring the slopes on the head surface might be a possible approach to determine the real mass model type.

5 Summary

A gravitation modeling method, LT-DI, is presented in this paper, and the analytical closed formulations of gravitational potential and attraction are derived. The LT-DI method shows the capacity to model the gravitation of irregular-shaped heterogeneous celestial bodies, in which case traditional methodologies are limited or fail. The theoretical analysis confirms the global convergence of our method (in both exterior and interior, and on the surface of the body). Using representative benchmark tests, and a running case of asteroid (25143)

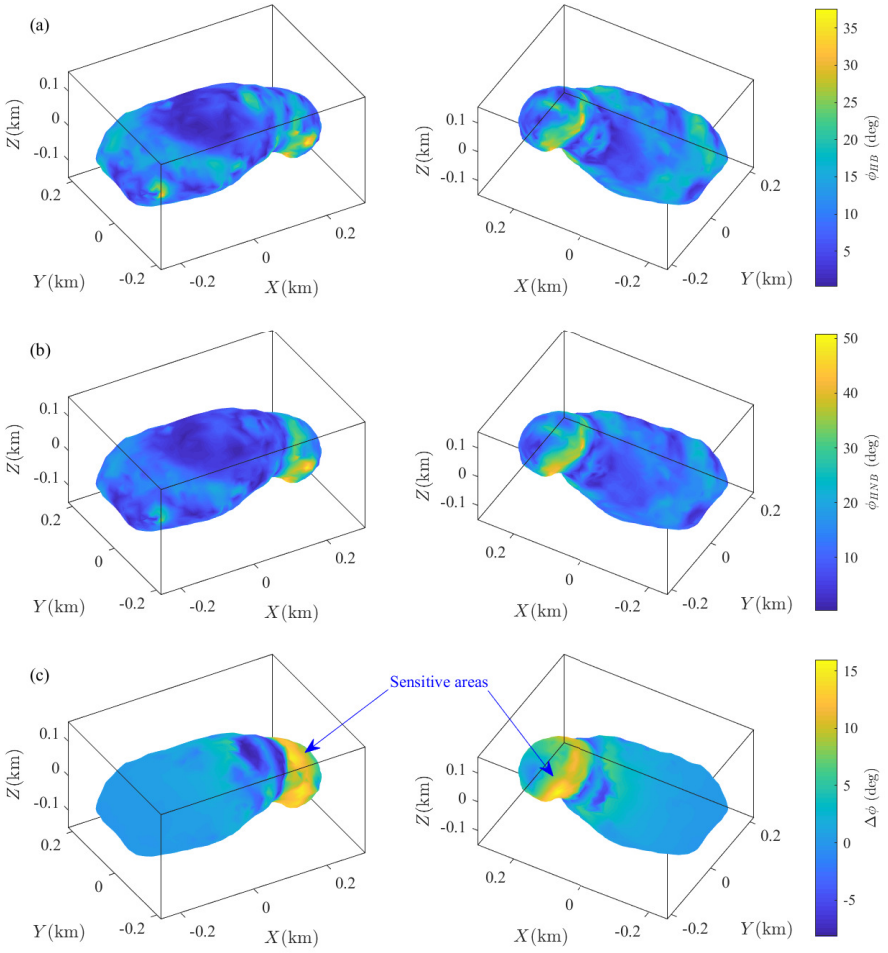

Fig. 10 (a) Local slopes on Itokawa's surface generated from H-B model (ϕ_{HB}). (b) Local slopes generated from H-N-B model (ϕ_{HNB}). (c) The difference between ϕ_{HNB} and ϕ_{HB} (here we present $\Delta\phi = \phi_{HNB} - \phi_{HB}$).

Itokawa, we prove that the proposed method is feasible and reliable in future studies of heterogeneous small bodies.

The LT-DI modeling formulation is the minimum gravitation representation on linear tetrahedral mesh. It treats the gravitation contribution from the surface and the interior density gradient respectively, providing flexibility and possibility of simplification. This FE-mesh-based formulation is naturally suitable to be migrated to the research on the morphology and dynamics of small bodies. The advantages of LT-DI make it a favourable choice in the following situations where traditional methods could fail:

1. the dynamics environment modeling on the surface of irregular heterogeneous bodies;
2. the interior gravitation modeling of heterogeneous bodies, which future asteroid missions may require;
3. the computation of gravitational interaction energy of celestial bodies, which is a critical index for stability analysis of gravitational aggregates [6].

As a prospective, for most of continuous systems without a clear boundary (a boundary where the density jumping occurs), such as average density models of the galaxy and interstellar dust, the density on the boundary of the mesh system is zero, which means the surface part is zero when applying LT-DI formulation. For these cases, only the interior part occurs in LT-DI formulation, which provides an outer scope extension of this method in astrophysics research.

Acknowledgments. The authors acknowledge financial support provided by the National Natural Science Foundation of China Grant No. 12022212 and No.11872223.

Author Contributions. YY, JFL and WYD devised the project and conceptual ideas. Technical details were completed by WYD, YY and HB. WYD performed the computational works. WYD and BC analysed computation results. The paper writing was completed by WYD, YY and BC. All authors approved of this manuscript.

Data Availability. All data used in this article are publicly accessible. High-resolution shape model of Itokawa can be obtained in NASA Planetary Data System.

References

[1] Abe, S., Mukai, T., Hirata, N., Barnouin-Jha, O. S., Cheng, A. F., Demura, H., . . . Yoshikawa, M. (2006). Mass and Local Topography Measurements of Itokawa by Hayabusa. Science, 312(5778), 1344-1347. doi:10.1126/science.1126272

[2] Conway, J. T. (2015). Analytical solution from vector potentials for the gravitational field of a general polyhedron. Celestial Mechanics and Dynamical Astronomy, 121(1), 17-38. doi:10.1007/s10569-014-9588-x

[3] D'Urso, M. G. (2014). Analytical computation of gravity effects for polyhedral bodies. Journal of Geodesy, 88(1), 13-29. doi:10.1007/s00190-013-0664-x

[4] D'Urso, M. G. (2014). Gravity effects of polyhedral bodies with linearly varying density. Celestial Mechanics & Dynamical Astronomy, 120(4), 349-372. doi:10.1007/s10569-014-9578-z

[5] D'Urso, M. G., & Trotta, S. (2017). Gravity Anomaly of Polyhedral Bodies Having a Polynomial Density Contrast. Surveys in Geophysics, 38(4), 781-832. doi:10.1007/s10712-017-9411-9

[6] Eriguchi, Y., Hachisu, I., & Sugimoto, D. (1982). Dumb-Bell-Shape Equilibria and Mass-Shedding Pear-Shape of Selfgravitating Incompressible Fluid. Progress of Theoretical Physics, 67(4), 1068-1075. doi:10.1143/PTP.67.1068

[7] Ermakov, A. I., Zuber, M. T., Smith, D. E., Raymond, C. A., Balmino, G., Fu, R. R., & Ivanov, B. A. (2014). Constraints on Vesta's interior structure using gravity and shape models from the Dawn mission. Icarus, 240, 146-160. doi:https://doi.org/10.1016/j.icarus.2014.05.015

[8] Fujiwara, A., Kawaguchi, J., Yeomans, D. K., Abe, M., Mukai, T., Okada, T., . . . Uesugi, K. (2006). The Rubble-Pile Asteroid Itokawa as Observed by Hayabusa. Science, 312(5778), 1330-1334. doi:doi:10.1126/science.1125841

[9] Fukushima, T. (2017). Precise and Fast Computation of the Gravitational Field of a General Finite Body and Its Application to the Gravitational Study of Asteroid Eros. The Astronomical Journal, 154(4), 145. doi:10.3847/1538-3881/aa88b8

[10] Gaskell, R., et al. (2008). Gaskell Itokawa Shape Model V1.0. HAY-A-AMICA-5-ITOKAWASHAPE-V1.0. NASA Planetary Data System.

[11] Hansen, R. O. (1999). An analytical expression for the gravity field of a polyhedral body with linearly varying density. GEOPHYSICS, 64(1), 75-77. doi:10.1190/1.1444532

[12] Hofmann-Wellenhof, B., & Moritz, H. (2006). Physical geodesy: Springer Science & Business Media.

[13] Holstein, H. (2003). Gravimagnetic anomaly formulas for polyhedra of spatially linear media. GEOPHYSICS, 68(1), 157-167. doi:10.1190/1.1543203

[14] Jänich, K., & Kay, L. (2001). Vector analysis: Springer.

[15] Jiang, Y., & Baoyin, H. X. (2016). Periodic Orbit Families in the Gravitational Field of Irregular-Shaped Bodies. The Astronomical Journal, 152(5), 137. doi:10.3847/0004-6256/152/5/137

[16] Lowry, S. C., Weissman, P. R., Duddy, S. R., Rozitis, B., Fitzsimmons, A., Green, S. F., . . . van Oers, P. (2014). The internal structure of asteroid (25143) Itokawa as revealed by detection of YORP spin-up. A&A, 562, A48. Retrieved from https://doi.org/10.1051/0004-6361/201322602

[17] Petrović, S. (1996). Determination of the potential of homogeneous polyhedral bodies using line integrals. Journal of Geodesy, 71(1), 44-52. doi:10.1007/s001900050074

[18] Romain, G., & Jean-Pierre, B. (2001). Ellipsoidal Harmonic expansions of the gravitational potential: Theory and application. Celestial Mechanics and Dynamical Astronomy, 79(4), 235-275. doi:10.1023/a:1017555515763

[19] Scheeres, D., Gaskell, R., Abe, S., Barnouin-Jha, O., Hashimoto, T., Kawaguchi, J., . . . Hirata, N. (2006). The actual dynamical environment about Itokawa. Paper presented at the AIAA/AAS Astrodynamics Specialist Conference and Exhibit.

[20] Scheeres, D. J., French, A. S., Tricarico, P., Chesley, S. R., Takahashi, Y., Farnocchia, D., . . . Lauretta, D. S. (2020). Heterogeneous mass distribution of the rubble-pile asteroid (101955) Bennu. Science Advances, 6(41), eabc3350. doi:doi:10.1126/sciadv.abc3350

[21] Tsoulis, D. (2012). Analytical computation of the full gravity tensor of a homogeneous arbitrarily shaped polyhedral source using line integrals. GEOPHYSICS, 77(2), F1-F11. doi:10.1190/geo2010-0334.1

[22] Tsoulis, D., & Petrović, S. (2001). On the singularities of the gravity field of a homogeneous polyhedral body. GEOPHYSICS, 66(2), 535-539. doi:10.1190/1.1444944

[23] Wei, B., & Shang, H. (2021). Global Gravity Field Modeling of Small Bodies with Heterogeneous Mass Distributions. Journal of Guidance, Control, and Dynamics, 1-14. doi:10.2514/1.G005945

[24] Werner, R. A. (1994). The gravitational potential of a homogeneous polyhedron or don't cut corners. Celestial Mechanics and Dynamical Astronomy, 59(3), 253-278. doi:10.1007/bf00692875

[25] Werner, R. A., & Scheeres, D. J. (1996). Exterior gravitation of a polyhedron derived and compared with harmonic and mascon gravitation representations of asteroid 4769 Castalia. Celestial Mechanics & Dynamical Astronomy, 65(3), 313-344.

[26] Wittick, P. T., & Russell, R. P. (2017). Mascon models for small body gravity fields. Paper presented at the AAS/AIAA Astrodynamics Specialist Conference.

[27] Wittick, P., & Russell, R., 2018, Hybrid Gravity Models for Kleopatra, Itokawa, and Comet 67P/C-G. in AAS/AIAA Astrodynamics Specialist Conference, (18).

[28] Yu, Y. (2016). Orbital dynamics in the gravitational field of small bodies: Springer.

[29] Yu, Y., Cheng, B., Hayabayashi, M., Michel, P., & Baoyin, H. (2019). A finite element method for computational full two-body problem: I. The mutual potential and derivatives over bilinear tetrahedron elements. Celestial Mechanics & Dynamical Astronomy, 131(11), 51. doi:10.1007/s10569-019-9930-4

[30] Yu, Y., Michel, P., Hirabayashi, M., Schwartz, S. R., Zhang, Y., Richardson, D. C., & Liu, X. (2018). The Dynamical Complexity of Surface Mass Shedding from a Top-shaped Asteroid Near the Critical Spin Limit. The Astronomical Journal, 156(2), 59. doi:10.3847/1538-3881/aaccf7